Multi-Proxy, Multi-Season Streamflow Reconstruction with Mass Balance Adjustment

Hung T.T. Nguyen[1], Stefano Galelli[1], Chenxi Xu[2,3], and Brendan M. Buckley[4]

[1]Pillar of Engineering Systems and Design, Singapore University of Technology and Design, Singapore
[2]Key Laboratory of Cenozoic Geology and Environment, Institute of Geology and Geophysics, Chinese Academy of Sciences, Beijing, China
[3]CAS Center for Excellence in Life and Paleoenvironment, Beijing, China
[4]Lamont-Doherty Earth Observatory, Columbia University, New York, USA

Key Points:

- Ring width and $\delta^{18}O$ are combined to reconstruct dry season, wet season, and annual streamflow
- Optimal proxy combinations are found with an automatic input selection scheme
- Mass-balance adjustment improves the agreement between seasonal and annual reconstructions

Corresponding author: Hung Nguyen, tanthaihung_nguyen@mymail.sutd.edu.sg

Abstract

Despite having offered important hydroclimatic insights, streamflow reconstructions still see limited use in water resources operations, because annual reconstructions are not suitable for decisions at finer time scales. Attempts towards sub-annual reconstructions have relied on statistical disaggregation, which uses none or little proxy information. Here, we develop a novel framework that optimizes proxy combinations to simultaneously produce seasonal and annual reconstructions. Importantly, the framework ensures that total seasonal flow matches annual flow closely. This mass balance criterion is necessary to avoid misguiding water management decisions, such as water allocation. Using the framework, and leveraging a multi-species network of ring width and cellulose $\delta^{18}O$ in Southeast Asia, we reconstruct seasonal and annual inflow to Thailand's largest reservoir. The reconstructions are statistically skillful. This work is one step closer towards operational usability of streamflow reconstruction in water resources management.

Plain Language Summary

Long history of river discharge, or streamflow, can be reconstructed from tree rings. These reconstructions help us understand the water cycle in the past, but they have not been widely used in water resources operations. This is because reconstructions are often annual (having only one data point per year). By combining different tree species and different features of tree rings (for example, ring width and stable isotope ratio), it is possible to reconstruct seasonal streamflow in addition to the annual one, and that is our first goal. But a major challenge arises: how do we ensure that the total flow volume of the seasonal reconstructions closely matches the annual one? This criterion is called mass balance, and it is important to avoid misguiding water management decisions such as allocating water to different sectors. We develop a novel method to reconstruct seasonal and annual streamflow while accounting for mass balance at the same time. Our work is thus a step closer towards operational usability of streamflow reconstructions in water resources management.

1 Introduction

Dendrohydrology, the study of past hydroclimate using tree rings, has been largely motivated by water resources management. The field traces back to Hardman and Reil (1936), who recognized that instrumental records were too short to understand drought trends, and demonstrated that better understanding could be gained from exploring the links between tree rings and streamflow. Their work was motivated by contemporary droughts that affected irrigation. Also to understand droughts, Schulman (1945) established a tree ring chronology for the Colorado River Basin, this time motivated by the war effort—to examine Hoover Dam's hydropower production reliability to meet wartime demand. While these early works stopped at studying tree ring indices, dendrohydrology took a big step when Stockton (1971), leveraging advanced multivariate techniques (Fritts et al., 1971), showed that reconstructing streamflow record back in time was feasible—long term surface water availability could now be quantified directly. Soon, multiple streamflow reconstructions were developed across the Colorado River Basin (Stockton & Jacoby, 1976), revealing the shortcomings of the Colorado River Compacts (Woodhouse et al., 2006), and providing insights about long term hydrology of Lake Powell, the United States' second largest reservoir.

Streamflow reconstruction has become "an important planning and research tool" in water resources management (Meko & Woodhouse, 2011). Yet, its use in practical, operational aspects of water management is still limited. That is because reconstructions often target specific components of the hydrograph that best correlated with tree ring proxies. Perhaps most commonly, reconstructions from ring width often target the growth season (e.g., D'Arrigo, Abram, et al., 2011; Güner et al., 2017). Another example is given by reconstructions targeting peak flow using tree ring cellulose stable oxygen isotope ratio ($\delta^{18}O$) (C. Xu et al., 2019). These reconstructions reveal important insights about the hydroclimate, but do not provide the total annual surface water availability. Other works target the annual flow (e.g., Rao et al., 2018; Nguyen & Galelli, 2018), but even so, the annual resolution is not suitable for making operational decisions at finer time scales—crop planning, for instance, is often based on seasonal flow; reservoir releases are determined at monthly or even weekly time steps.

The water resources community recognizes the need for sub-annual reconstructions. Attempts towards this goal have relied on statistical disaggregation, assuming some statistical relationships between the sub-annual and annual flows (Prairie et al., 2008; Sauchyn & Ilich, 2017). These assumptions are reasonable but not always valid (Figure S1). More importantly, paleoclimatic proxies are not used in these methods, and their rich information are not utilized. Recent progress was made by Stagge et al. (2018), who used multispecies chronologies as additional inputs to disaggregation, showing that these inputs can be weighted differently for each month to improve the monthly reconstructions.

The works of Stagge et al. (2018), C. Xu et al. (2019), and others discussed above suggest that different proxies have different seasonal sensitivities. Therefore, instead of disaggregation, we propose to use multiple proxies to simultaneously reconstruct sub-annual (e.g., seasonal) and annual flows. Two challenges arise. How to combine prox-

ies optimally for different targets? And how to ensure that the seasonal flows add up to the annual flow, i.e., how to account for mass balance? We develop a unified framework to address both challenges. Mass balance is accounted for by a term in the regression formulation that penalizes the differences between total seasonal flow and annual flow (Section 3.1), and proxy combination is optimized with an automatic input selection scheme (Section 3.2). We test the framework with a case study in the Chao Phraya River Basin, Thailand, pooling together a multi-species network of ring width and cellulose $\delta^{18}O$ chronologies from Southeast Asia (Section 2). This work is one step closer towards operational usability of streamflow reconstruction in water resources management.

2 Study Site and Data

2.1 The Southeast Asian Dendrochronology Network

Over the past three decades, an extensive network of tree ring chronologies have been developed in Southeast Asia. This network has been instrumental in improving our understanding of Southeast Asia's hydroclimate and history. Tree ring data from Thailand and northern Vietnam (Buckley, Palakit, et al., 2007; Sano et al., 2009) revealed a multidecadal drought, what is later known as the Strange Parallel Droughts (E. R. Cook et al., 2010), which coincided with a tumultuous period of Southeast Asian history (Lieberman, 2003; Lieberman & Buckley, 2012). Further back in time, tree ring data from southern Vietnam linked megadroughts in the 14^{th} and 15^{th} centuries to the demise of the Angkor Civilization (Buckley et al., 2010, 2014). These findings are among many insights that the Southeast Asian Dendrochronology Network has brought forth.

In this work, we use twenty tree ring chronologies from Vietnam, Laos, Cambodia, Thailand, and Myanmar (Figure 1). The chronologies at Kirirom, Petchaburi, Pha Taem, and Wiang Haeng are published here for the first time. The metadata of the chronologies are provided in Table 1. The common period of most chronologies in our network is 1748–2005 (Figure S6), and is the same as the time span of our $\delta^{18}O$ network. Several chronologies are some decades shorter. Following Stagge et al. (2018), we imputed the missing years using the R package `missMDA` (Josse & Husson, 2016) (see Figure S7). We imputed the tree ring data instead of building nested models because nesting is not applicable in our reconstruction framework. As we shall explain in Section 3.1, the framework is designed to account for mass balance, tuning the regression parameters such that the total sub-annual flow matches the annual flow closely. With nesting, the final variance correction can disrupt the mass balance.

2.2 Cellulose $\delta^{18}O$

We use four chronologies of tree ring cellulose stable oxygen isotope ratio ($\delta^{18}O$) that were developed in Laos, Thailand, and Vietnam over the past decade (Figure 1 and Table 2). $\delta^{18}O$ exhibits strong mechanical and statistical relationship with the hydroclimate (C. Xu et al., 2011; Sano et al., 2012), and has been used to reconstruct wet season precipitation in the region (C. Xu et al., 2015, 2018). $\delta^{18}O$ in Laos was also found

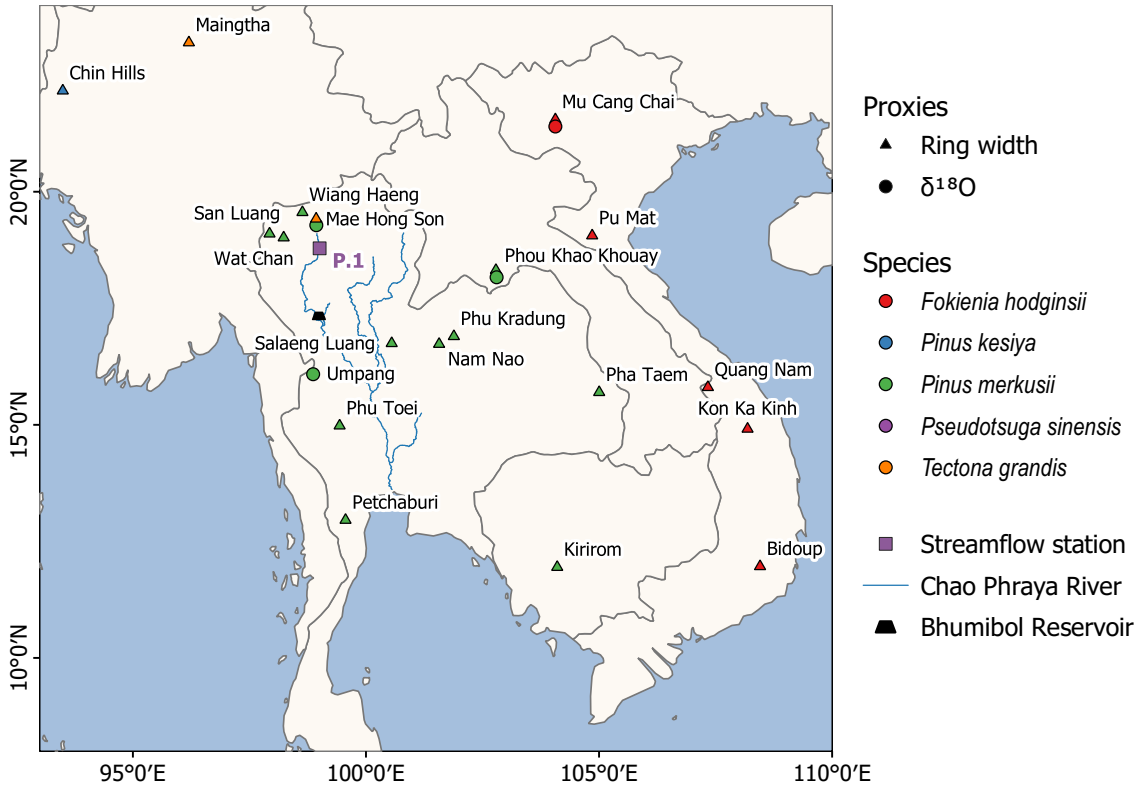

Figure 1. Map of the study region, showing the Chao Phraya River, the proxy network, and the target streamflow station.

to have significant negative correlation with Mekong River water level (C. Xu et al., 2013), suggesting promising hydrological applications. Finally, three $\delta^{18}O$ chronologies were used to reconstruct Chao Phraya River peak season flow (C. Xu et al., 2019). These works support recent literature (Treydte et al., 2006; G. Xu et al., 2019) that $\delta^{18}O$ has indeed moved beyond "potential" (Gagen et al., 2011), and earned its place as a practical, valuable paleoclimate proxy.

2.3 Streamflow

The Chao Phraya River Basin covers 30% of Thailand's area, and is home to about 25 million people. Thailand's largest reservoir, the Bhumibol (active capacity 9.7 km^3), lies on the Ping River tributary. Reliable operations of this reservoir require accurate assessment of inflow availability, on both inter- and intra-annual scales.

Streamflow station P.1 is located upstream of Bhumibol Reservoir. P.1 has the longest and most complete record in Thailand: daily data are available from April 1921–present. Since 1985, the river upstream of P.1 has been impounded by the Mae Ngat Dam, which, at full capacity, stores about 14% of P.1's mean annual flow. Dam operations modify the seasonal streamflow patterns, thereby interfering with the proxy-streamflow relationship. Therefore, we naturalized the streamflow data from 1985. The naturalization process is

Table 1. Metadata of tree ring width chronologies.

Site	Longitude	Latitude	Species	References
Bidoup	108.45	11.97	*Fokienia hodginsii*	Buckley et al. (2010)
Chin Hills	93.50	22.17	*Pinus kesiya*	Rao (2020)
Kim Hy	106.04	22.25	*Pseudotsuga sinensis*	Hansen et al. (2017)
Kirirom	104.10	11.95	*Pinus merkusii*	This study[a]
Kon Ka Kinh	108.18	14.91	*Fokienia hodginsii*	Buckley et al. (2019)
Mae Hong Son	98.93	19.28	*Tectona grandis*	Buckley, Palakit, et al. (2007)
Maingtha	96.20	23.20	*Tectona grandis*	D'Arrigo, Palmer, et al. (2011)
Mu Cang Chai	104.06	21.40	*Fokienia hodginsii*	Sano et al. (2009)
Nam Nao	101.57	16.73	*Pinus merkusii*	Buckley et al. (1995)
Petchaburi	99.56	12.96	*Pinus merkusii*	This study
Pha Taem	105.00	15.70	*Pinus merkusii*	This study
Phou Khao Khouay	102.79	18.32	*Pinus merkusii*	Buckley, Duangsathaporn, et al. (2007)
Phu Kradung	101.88	16.90	*Pinus merkusii*	D'Arrigo et al. (1997)
Phu Toei	99.43	14.98	*Pinus merkusii*	E. R. Cook et al. (2010)
Pu Mat	104.85	19.06	*Fokienia hodginsii*	Buckley et al. (2019)
Quang Nam	107.33	15.81	*Fokienia hodginsii*	Buckley et al. (2017)
Salaeng Luang	100.55	16.75	*Pinus merkusii*	Buckley et al. (1995)
San Luang	97.93	19.10	*Pinus merkusii*	E. R. Cook et al. (2010)
Wat Chan	98.23	19.02	*Pinus merkusii*	Buckley et al. (1995)
Wiang Haeng	98.64	19.56	*Pinus merkusii*	This study

[a] Several cores from this site were analyzed by Zhu et al. (2012) for $\delta^{18}O$ but the ring width chronology has not been published until now.

Table 2. Metadata of $\delta^{18}O$ chronologies.

Site	Longitude	Latitude	Species	References
Mae Hong Son	98.93	19.28	*Pinus merkusii*	C. Xu et al. (2015)
Mu Cang Chai	104.06	21.40	*Fokienia hodginsii*	Sano et al. (2012)
Phou Khao Khouay	102.79	18.32	*Pinus merkusii*	C. Xu et al. (2019)
Umpang	98.87	16.09	*Pinus merkusii*	C. Xu et al. (2018)

described in Text S3. After naturalization, we aggregated daily data into dry season (November–June), wet season (July–October), and water year (November–October). The season delineation was determined by the method of B. I. Cook and Buckley (2009) (Text S2). To match the proxies' time span, we finally used the streamflow data from November 1921 to October 2005.

2.4 Proxy–Streamflow Correlations

As a preliminary investigation, we performed correlation analyses between streamflow and proxy data. Correlations are calculated at different lags: $l = -2$ to $+2$ years. Negative lags account for the case when trees use stored carbon from previous years, and positive lags for the case when the catchment's runoff processes are slower than precipitation inputs (Stockton & Jacoby, 1976; Meko et al., 2007). For robustness, we repeated the correlation analysis 1,000 times using the stationary bootstrap (Politis & Romano, 1994). In the following discussion we refer to the median bootstrap correlations (Figure 2).

Among the ring width sites, there are multiple correlation patterns (Figure 2a): some sites such as Chin Hills and Phu Toei correlate positively, while others (e.g., Phou Khao Khouay) correlate negatively. Peculiarly, the Mae Hong Son site displays significant negative correlation at $l = -2$ but significant positive correlations at $l = 0$ and $l = 2$. Five sites do not correlate with streamflow at all. These various patterns suggest that the ring width–streamflow relationship is complex and "noisy". A large number of sites are thus required to extract the strongest signals.

Unlike ring width, $\delta^{18}O$ displays more consistent correlation patterns (Figure 2b): all significant correlations are negative, and the strongest correlations are often observed at $l = 0$. Some correlations have magnitudes larger than 0.5, while the largest correlation magnitude in ring width is only 0.36. These observations corroborate that $\delta^{18}O$ chronologies may contain stronger climate signals than do ring width chronologies (C. Xu et al., 2019; Gagen et al., 2011).

In general, we observe that ring width tends to correlate more strongly with dry season flow than with wet season flow. Conversely, $\delta^{18}O$ tends to correlate more strongly with wet season flow than with dry season flow. Both proxies correlate well with annual flow. The proxy-streamflow correlations observed here are also in agreement with the proxy-precipitation correlation analysis (Text S5). Both analyses show that tree ring proxies have different strength and sensitivity to different parts of the hydrograph, and have the potential to be combined for better seasonal reconstructions.

3 Reconstruction Framework

The correlation analysis shows diverse seasonal sensitivity among proxy chronologies and at different lags. To build reconstruction models, we define an *input* as a chronology–lag combination that significantly correlates with streamflow. For instance, some inputs for the annual reconstruction are Chin Hills ring-width at lag -2, and Umpang $\delta^{18}O$ at lag 0 (Figure 2).

The reconstruction framework consists of two main modules: Regression and Input Selection. In Regression (Section 3.1), the selected inputs for each target are given, and we find the regression coefficients that best match the targets while accounting for mass balance simultaneously, using a *penalized least squares* formulation. In Input Selection (Section 3.2), we find the best subset of inputs that minimizes the penalized least

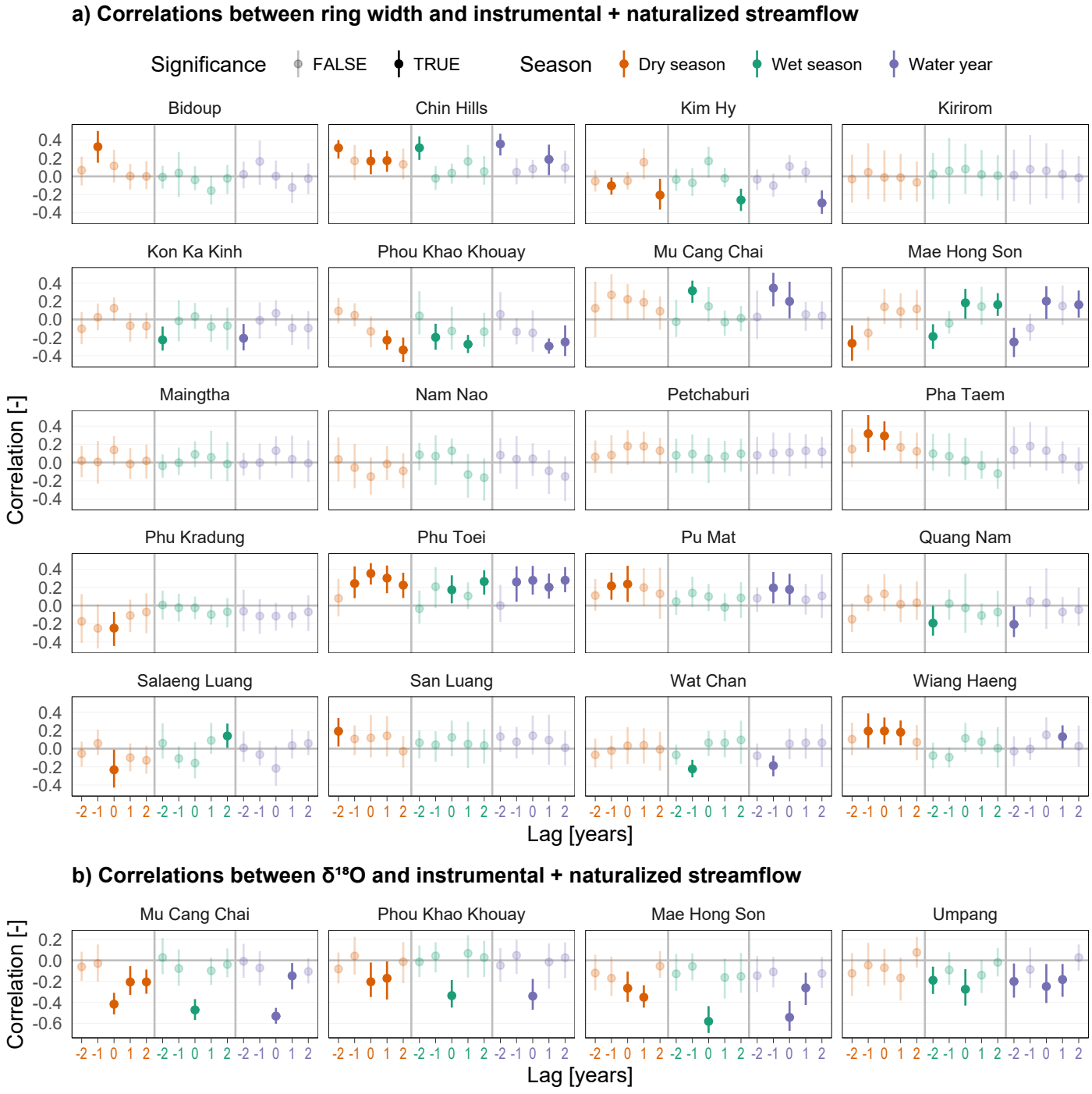

Figure 2. Streamflow–proxy correlations. The error bars show the 5$^{\text{th}}$–95$^{\text{th}}$ bootstrapped empirical quantiles obtained from 1,000 replicates, using the stationary bootstrap (Politis & Romano, 1994). The dots indicate the medians. Lag l denotes correlations between proxy at year t and streamflow at year $t + l$.

squares. The two modules are unified in a nested optimization framework that includes a rigorous cross-validation scheme to assess reconstruction skills (Section 3.3).

3.1 Mass-balance-adjusted Regression

Assume that we have a matrix $\mathbf{U_d}$ whose columns contain the selected inputs for the dry season. We first need to remove multicollinearity within $\mathbf{U_d}$. A common approach in dendrohydrology is to perform Principal Component Analysis (PCA) on $\mathbf{U_d}$, then reduce the set of principal components (PCs) to a parsimonious subset that is most relevant to the streamflow target (Hidalgo et al., 2000; Coulthard et al., 2016). Here, we use a backward stepwise PC selection routine (Woodhouse et al., 2006). This transformation from the selected inputs to the selected PCs is denoted as the function $g(.)$:

$$\mathbf{X_d} = g(\mathbf{U_d}) \tag{1}$$

Similarly, given the selected inputs $\mathbf{U_w}$ for the wet season and $\mathbf{U_q}$ for the water year, we apply $g(.)$ to get

$$\mathbf{X_w} = g(\mathbf{U_w}) \tag{2}$$

$$\mathbf{X_q} = g(\mathbf{U_q}) \tag{3}$$

Now, let $\mathbf{y_d}, \mathbf{y_w}$, and $\mathbf{y_q}$ be the target time series of dry season, wet season, and annual streamflow, respectively (these targets can be log-transformed when necessary). Reconstructing streamflow for the three targets means solving the following regression equations:

$$\mathbf{y_d} = \mathbf{X_d}\boldsymbol{\beta_d} + \boldsymbol{\varepsilon_d} \tag{4}$$

$$\mathbf{y_w} = \mathbf{X_w}\boldsymbol{\beta_w} + \boldsymbol{\varepsilon_w} \tag{5}$$

$$\mathbf{y_q} = \mathbf{X_q}\boldsymbol{\beta_q} + \boldsymbol{\varepsilon_q} \tag{6}$$

where $\boldsymbol{\beta_d}, \boldsymbol{\beta_w}$, and $\boldsymbol{\beta_q}$ are the corresponding regression coefficients; and $\boldsymbol{\varepsilon_d}, \boldsymbol{\varepsilon_w}$, and $\boldsymbol{\varepsilon_q}$ are white noise.

Next, let

$$\mathbf{y} = \begin{bmatrix} \mathbf{y_d} \\ \mathbf{y_w} \\ \mathbf{y_q} \end{bmatrix}, \quad \mathbf{X} = \begin{bmatrix} \mathbf{X_d} & & \\ & \mathbf{X_w} & \\ & & \mathbf{X_q} \end{bmatrix}, \quad \boldsymbol{\beta} = \begin{bmatrix} \boldsymbol{\beta_d} \\ \boldsymbol{\beta_w} \\ \boldsymbol{\beta_q} \end{bmatrix}, \quad \text{and} \quad \boldsymbol{\varepsilon} = \begin{bmatrix} \boldsymbol{\varepsilon_d} \\ \boldsymbol{\varepsilon_w} \\ \boldsymbol{\varepsilon_q} \end{bmatrix}. \tag{7}$$

Equations 4–6 can then be converted to a more compact form

$$\mathbf{y} = \mathbf{X}\boldsymbol{\beta} + \boldsymbol{\varepsilon}. \tag{8}$$

Equation 8 has the canonical form of linear regression. It can be solved as a least-squares problem:

$$\min_{\boldsymbol{\beta}} \quad J_1 = (\mathbf{y} - \mathbf{X}\boldsymbol{\beta})'(\mathbf{y} - \mathbf{X}\boldsymbol{\beta}), \tag{9}$$

yielding the solution

$$\boldsymbol{\beta} = (\mathbf{X}'\mathbf{X})^{-1}\mathbf{X}'\mathbf{y}. \tag{10}$$

Solving Equation 8 is equivalent to solving Equations 4–6 simultaneously. The three regression problems in Equations 4–6 are independent of one another, and the above formulation places no constraints to match the sum of the seasonal flows to the annual flow. Therefore, such formulation can yield large differences in the annual mass balance. As we shall see later, this happens at station P.1.

To account for mass balance, it is tempting to impose a constraint,

$$\mathbf{X_d}\boldsymbol{\beta_d} + \mathbf{X_w}\boldsymbol{\beta_w} = \mathbf{X_q}\boldsymbol{\beta_q}. \tag{11}$$

But, Equation 11 is often overdetermined: it is a system of T equations, one for each year, and we almost always have more equations than unknowns in a regression problem. Instead, we can add to the objective function in Equation 9 a penalty term that is based on the differences ($\boldsymbol{\delta}$) between the LHS and the RHS of Equation 11.

$$\boldsymbol{\delta} = \mathbf{X_d}\boldsymbol{\beta_d} + \mathbf{X_w}\boldsymbol{\beta_w} - \mathbf{X_q}\boldsymbol{\beta_q}. \tag{12}$$

If the reconstructions involve log-transformed flows, the mass difference is

$$\delta_t = \log\Big(\exp(\mathbf{x_{d},}_t\boldsymbol{\beta_d}) + \exp(\mathbf{x_{w},}_t\boldsymbol{\beta_w})\Big) - \mathbf{x_{q},}_t\boldsymbol{\beta_q} \qquad \forall t = 1, ..., T. \tag{13}$$

Just as we minimize the squared differences between prediction and observation, we also minimize the squared mass differences. Finally, we add a weight λ to represent the importance of the penalty term, and obtain a new objective function

$$\min_{\boldsymbol{\beta}} \quad J_2 = (\mathbf{y} - \mathbf{X}\boldsymbol{\beta})'(\mathbf{y} - \mathbf{X}\boldsymbol{\beta}) + \lambda\boldsymbol{\delta}'\boldsymbol{\delta} \tag{14}$$

We call this the *penalized least squares* problem. Observe that when $\lambda = 0$, the penalty term disappears, and the penalized least squares problem becomes the canonical least squares problem. The higher λ is, the more important the penalty becomes.

Without flow transformation, $\boldsymbol{\delta}$ is linear (Equations 12), so J_2 is quadratic. We can solve Equation 14 analytically to get

$$\boldsymbol{\beta} = (\mathbf{X}'\mathbf{X} + \lambda\mathbf{A}'\mathbf{A})^{-1}\mathbf{X}'\mathbf{y} \tag{15}$$

where $\mathbf{A} = [\mathbf{X_d} \quad \mathbf{X_w} \quad -\mathbf{X_q}]$. The proof is provided in Text S6.

When log-transformations are involved, $\boldsymbol{\delta}$ is not linear, and Equation 14 cannot be solved analytically. But it can be solved numerically using any nonlinear solver. Here, we use an efficient quasi-Newton method called L-BFGS-B (Byrd et al., 1995), available in the R function `optim()`. We have implemented the mass-balance-adjusted regression procedure in the R package `mbr`, currently available on GitHub at `github.com/ntthung/mbr`.

3.2 Optimal Input Selection

A consolidated approach to input selection in the literature is to use Branch and Bound algorithms, such as Leaps and Bounds (Furnival & Wilson, 1974) or its more recent variants (Duarte Silva, 2001, 2002). These algorithms are conceived to balance goodness-of-fit with model simplicity. In this work however, we also need to account for mass balance besides goodness-of-fit. Therefore, the input selection routine must explicitly account for the penalized least squares objective (Equation 14). If the number of inputs

is small, we can exhaustively search all possible subsets and choose the one that yields the minimum penalized least square value (PLSV). However, this method quickly becomes infeasible with increasing input size: there are 2^n subsets of n inputs (for station P.1, $n = 19$, 28, and 30). A computationally tractable optimization is necessary (Galelli et al., 2014).

We formulate input selection as a binary optimization problem. Each input has an index, and a binary vector $\mathbf{p}$ encodes input selection: $p_i = 1$ means the i^{th} input is selected. For any given $\mathbf{p}$, i.e, for any given input subset, we can solve the mass-balance-adjusted regression problem to obtain a PLSV. Our goal then is to find $\mathbf{p}$ that has the best PLSV over all $\mathbf{p}$'s.

Note that $\mathbf{p}$ has three components: $\mathbf{p} = [\mathbf{d} \quad \mathbf{w} \quad \mathbf{q}]'$. Component $\mathbf{d}$ represents the dry season:

$$d_i = \begin{cases} 1 & \text{if proxy } i \text{ is used for the dry season} \\ 0 & \text{otherwise} \end{cases} \qquad i = 1, ..., n_d. \tag{16}$$

So, where $d_i = 1$, we take the i^{th} inputs and place into the matrix $\mathbf{U_d}$. Similarly, we create $\mathbf{U_w}$ from $\mathbf{w}$ and $\mathbf{U_q}$ from $\mathbf{q}$. Once we have $\mathbf{U_d}$, $\mathbf{U_w}$, and $\mathbf{U_q}$, the mass-balance-adjusted regression procedure can be applied. To improve the robustness of the input selection, the regression is cross-validated 50 times (Section 3.3), each yields one PLSV estimate. The average of all runs, denoted $f(\mathbf{p})$, is used as the final PLSV for $\mathbf{p}$.

The remaining task is to solve

$$\min_{\mathbf{p}} \; f(\mathbf{p}). \tag{17}$$

We solve Equation 17 with Genetic Algorithm (Holland, 1975), a metaheuristic optimization technique that allows us to treat the underlying regression as a black-box while searching for the best subset of inputs (Kohavi & John, 1997), and is well suited for binary optimization (Whitley, 1994). We use the R package `GA` (Scrucca, 2013). Details about the implementations are provided in Text S8.

3.3 Model Assessment

We set up a reconstruction experiment involving two models: Model 0 runs without the mass balance adjustment ($\lambda = 0$ in Equation 14) and Model 1 has the adjustment ($\lambda = 1$). Other than the different values for λ, both models are trained exactly the same way, following Sections 3.1 and 3.3.

During optimization, multiple reconstructions are created while the optimal $\mathbf{p}$ is sought for each model. These reconstructions are assessed with the PLSV. The final reconstructions, created with the optimal inputs, are further assessed post hoc with the commonly used metrics: coefficient of determination (R^2), reduction of error (RE), and coefficient of efficiency (CE) (Nash & Sutcliffe, 1970; Fritts, 1976). All metrics are calculated over 50 cross-validation runs.

Following Nguyen et al. (2020), we adopt a leave-25%-out cross-validation scheme, where each hold-out chunk is contiguous. The contiguous chunks aim to test whether

the reconstruction can capture regimes in the time series, in line with the traditional split-sample scheme. The 50 repetitions provide a distribution for each skill metric, allowing more robust estimation of the mean skill score. More importantly, the distributions enable us to assess the statistical significance of skills. For example, a reconstruction is considered statistically skillful with respect to CE at $\alpha = 0.1$ if the probability of negative CE is less than 0.1.

4 Results

4.1 Reconstructions

For Model 0's dry season and annual reconstructions, all metrics are at least 0.40, and the reconstructions match their targets closely (Figure 3a). Furthermore, these reconstructions are statistically skillful at $\alpha = 0.1$. Conversely, Model 0's wet season reconstruction is not statistically skillful. Although the mean RE and CE are positive (RE = 0.35, CE = 0.23), these scores vary widely over the cross-validation runs (Figure S12), suggesting that the wet season reconstruction is sensitive to training data. The large variability of skills is also consistent with the high variability of streamflow (Figure S5). These observations suggest that there may be nonlinearity in the streamflow–proxy relationships at the extremes. In future studies, nonlinear reconstruction models (e.g., Nguyen & Galelli, 2018) could be incorporated to address this problem.

Model 1, with the penalty term, makes visible adjustments to the seasonal reconstructions but minimal changes to the annual one for the instrumental period (Figure 3a). Dry season skills slightly decrease, wet season's RE and CE increase, and annual skills remain almost the same. While the mean skill scores of both models are similar, Model 1 produces notably narrower distributions of RE and CE for the wet season (Figure S12). Consequently, Model 1's wet season reconstruction becomes statistically skillful. Overall, Model 1 is more robust.

To understand Model 1's robustness, let us recall the models' formulation. Model 0 reconstructs the dry season, wet season, and annual flows independently. Each reconstruction is geared towards its own target, and can become sensitive to training data—the wet season reconstruction does. Contrarily, Model 1 links all three reconstructions together via the penalty term (Equations 12–14). This link provides each reconstruction with additional information from the other two, thus preventing each reconstruction from overfitting to its own target. In our case, the wet season reconstruction benefited significantly from this additional information to become statistically skillful, with minimal trade-off from the other two reconstructions.

The selected input subsets by both models provide further insights into their similarities and differences. Both models use similar input subsets, with identical ones for the water year. However, Model 1 uses fewer inputs than does Model 0 for the wet and dry seasons (Figure 4). Therefore, the models behave similarly, but Model 1 is more parsimonious.

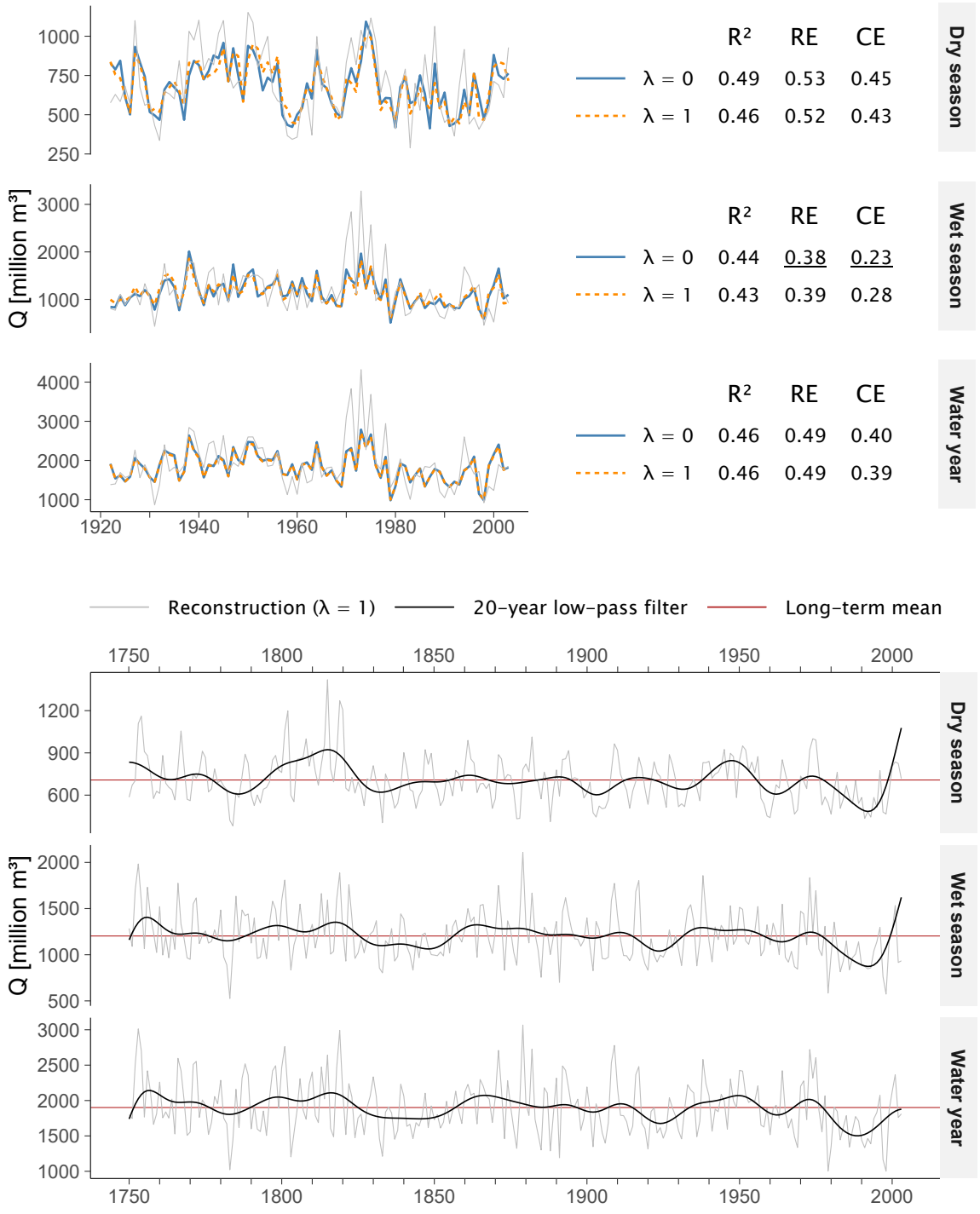

Figure 3. (a) Reconstruction skills and time series for the instrumental period, produced using two models: without mass balance penalty ($\lambda = 0$) and with penalty ($\lambda = 1$) in the regression problem (Equation 14). Grey lines show naturalized observations. Underlined scores show where the reconstruction is not statistically skillful at $\alpha = 0.1$. (b) Full reconstructions with $\lambda = 1$.

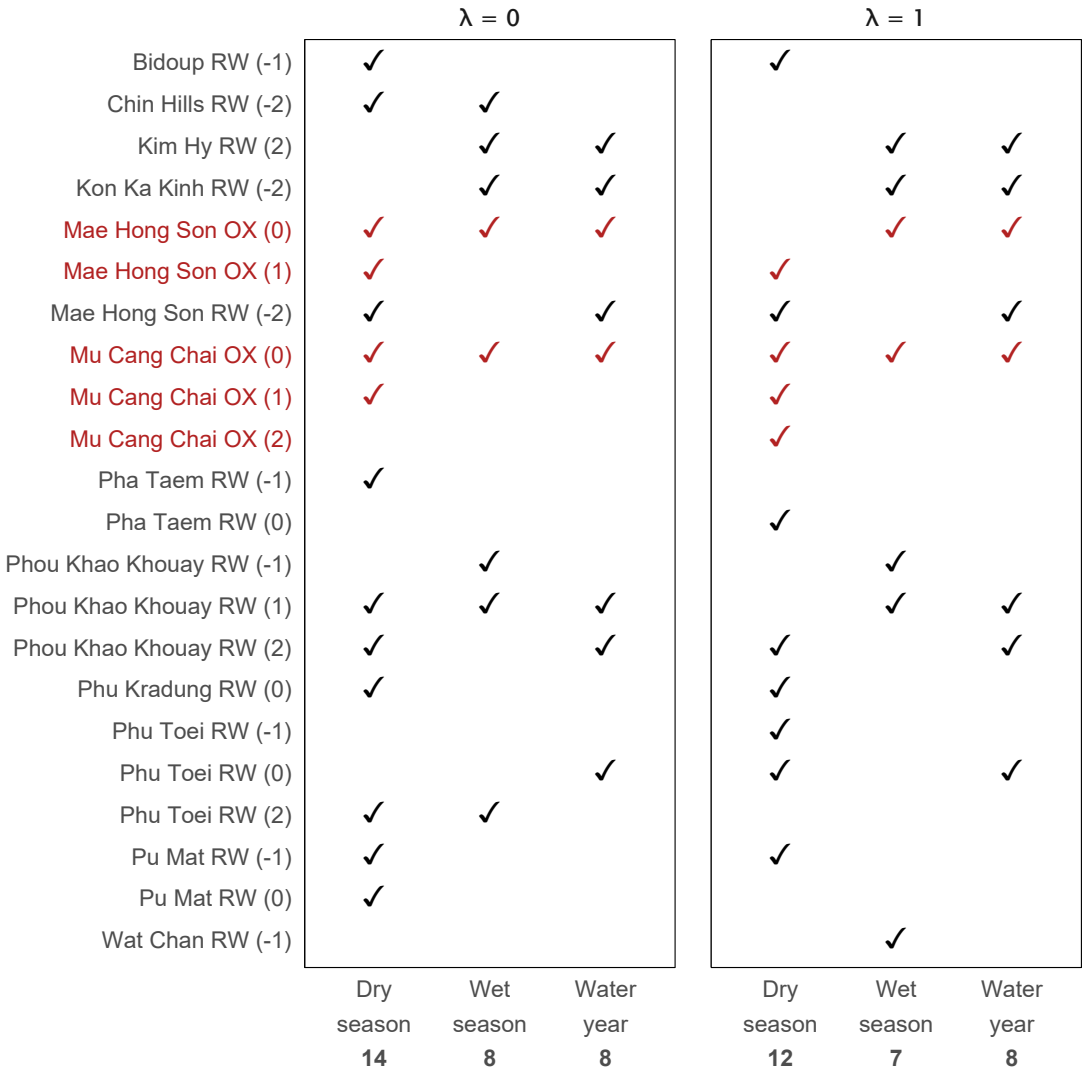

Figure 4. Selected inputs for each streamflow target (columns) in each models (panels). Only inputs that were selected at least once are shown. The stable oxygen isotope (OX) inputs are marked in dark red. Bold numbers at the bottom row of the x-axis are the number of selected inputs in each column.

Surprisingly, the Mu Cang Chai and Mae Hong Son $\delta^{18}O$ chronologies were consistently selected by both models for all reconstructions, including the dry season reconstructions where we expected ring width chronologies to dominate, based on the observed tendencies of ring width to correlate more with wet season flow and $\delta^{18}O$ to correlate more with dry season flow. Upon closer examinations of the correlation analysis (Figure 2), the puzzle is solved. First, the $\delta^{18}O$ chronologies are intercorrelated (C. Xu et al., 2019), and the input selection algorithm correctly selected the two sites that exhibit the strongest correlations. Second, while these $\delta^{18}O$ chronologies correlate less with dry

season flow than they do with wet season flow, the correlations are still stronger than those observed at many ring width sites.

Over the whole study horizon, we observe similar results to those of the instrumental period (Figure S13). The two models agree with each other. Model 1's adjustments are generally small. The largest adjustments are in the wet season (± 400 Mm^3); smaller but notable adjustments are seen in the dry season (± 200 Mm^3), and minute adjustments (< 90 Mm^3) are seen in the annual reconstruction. We will examine the effects of these adjustments in Section 4.2.

The reconstructions provide some interesting insights into the inter- and intra-annual variability of the river (Figure 3b). Between 1825–1855, sustained low flow was observed in the wet season and water year reconstructions. However, in the dry season, the low flow period ended 15 years earlier, around 1840. Conversely, a period of sustained high flow was observed in all three reconstructions between 1790–1820, especially for the dry season. Most notably, dry season flow in 1815 was so high that it accounted for more than 50% of the annual flow—a rare event that occurred in only 8 of 254 years (Figure S14, see also Text S9).

4.2 Annual Mass Balance

For each model, we compare the total seasonal flow with the annual flow. To preserve the annual mass balance, these two time series should ideally be the same. However, for Model 0, large discrepancies are seen between the two time series (Figure 5a). For Model 1, the two time series agree with each other better. As each time series provides an estimate of the annual water budget, we are also interested in their distributions. We observe that the distributions produced by Model 0 are notably different from each other, but those produced by Model 1 are almost identical (Figure 5b). This implies that the distributions derived from Model 1 are more reliable. Using the same analysis, we show that Model 1 also produces more reliable distributions of the dry and wet season's water budget than does Model 0 (Figure S15).

Next, for each model, we calculate the mass difference, ΔQ, between the total seasonal flow and the annual flow, then examine its trajectory and distribution (Figures 5c and 5d). The mass difference for Model 0 ranges from -640 Mm^3 to 600 Mm^3, while that range for Model 1 is -270 Mm^3 to 370 Mm^3; a 50% reduction in range. Moreover, Model 0 yields a mass difference outside the interval ± 190 Mm^3 ($\pm 10\%$ of the mean annual flow; shaded region in Figure 5d) in 28% of the years. That figure for Model 1 is only 11%. By these metrics, Model 1 is twice better than Model 0 in terms of preserving mass balance.

5 Discussion and Conclusions

In Section 4.1, we showed that the optimal input selection procedure yields good reconstruction skills for both model setups, and that Model 1, by imposing a mass balance adjustment, produces more robust reconstructions than does Model 0. More im-

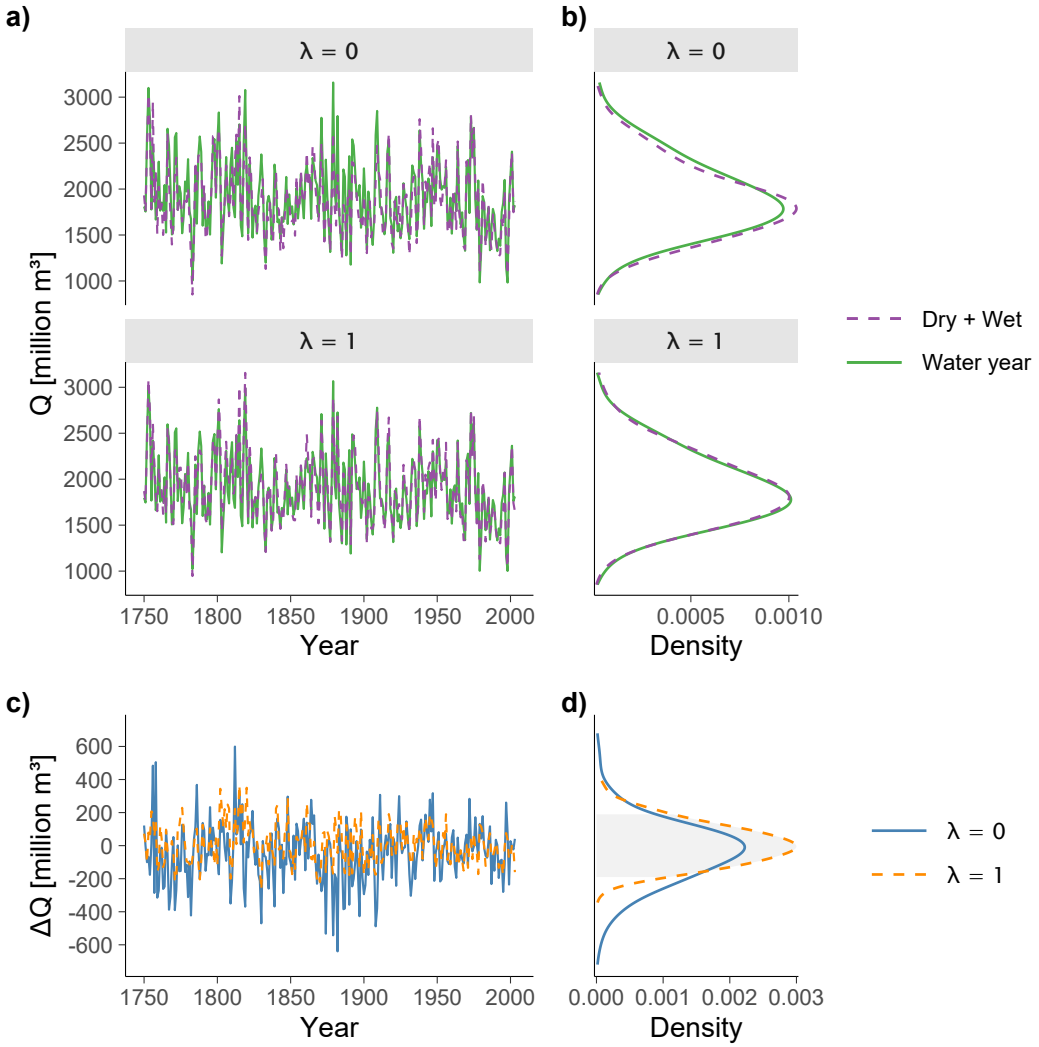

Figure 5. (a) Comparison between the total seasonal flow (TSF; Wet + Dry) and the annual flow (AF; Water year) for Model 0 ($\lambda = 0$) and Model 1 ($\lambda = 1$). (b) Distributions of the annual water budget, estimated by either the TSF or the AF for both models. (c) The differences, ΔQ, between the TSF and the AF. (d) Distributions of ΔQ. The shaded region denotes the ± 190 Mm^3 range, equivalent to $\pm 10\%$ of the mean annual flow.

portantly, the adjustment significantly reduces the differences between the total seasonal flow and the annual flow (Section 4.2). Without the adjustment, the mass difference can be as large as 640 Mm^3, or about 30% of the mean annual flow. It amounts to 90% of the irrigation demand from the Ping River downstream of Bhumibol Reservoir (Divakar et al., 2011). Such a discrepancy may lead to water allocation disputes. With the adjustment, both the frequency and magnitude of discrepancies are reduced—this is crucial for water availability assessment, a major goal of dendrohydrology.

We also showed that the mass-balanced-adjusted regression produces reliable distributions of the seasonal and annual streamflow. These distributions can be used for probabilistic studies in water resources applications. For example, sub-annual stochastic time series can be generated from the distributions to be used in bottom-up vulnerability assessments of water systems (Pielke et al., 2012; Herman et al., 2016). In Text S10 we illustrate one simple way to do so (by sampling from a bivariate distribution fitted to the seasonal reconstructions), but more advanced methods are available (e.g., Borgomeo, Farmer, & Hall, 2015; Borgomeo, Pflug, et al., 2015).

The framework that we proposed here can be reapplied and expanded in several ways. First, analysts adopting our framework have the choice to tune λ, depending on how important it is to preserve mass balance in their applications. In this case, a sensitivity analysis with respect to λ may be informative. Second, the mass balance formulation is applicable to other climate variables such as precipitation, and to other contexts where a penalty term in the regression equation is desirable. For example, if one wishes to reconstruct streamflow at two tributaries as well as the main stream of a river, the mass balance adjustment should be used to minimize the difference between the total flow of the tributaries and the flow on the main stream. Finally, the mass balance formulation is readily extendable to higher resolutions, e.g., quarterly or monthly (Text S7), as long as the proxy network is sensitive enough to the higher resolution targets. These directions can help dendrohydrology realize its value in operational water management, an area where annual, unconstrained streamflow reconstructions have had limited success.

Acknowledgments

We are indebted to Edward Cook for the updated chronologies (Salaeng Luang, Mae Hong Son, and Mu Cang Chai), and for his valuable comments. We are also grateful to Thanh Dang for the VIC-Res model output. The diligent work of Le Canh Nam and many other local colleagues in collecting tree core samples over many years is crucial in building the tree ring network, and is sincerely appreciated. We knew of Hardman and Reil (1936) through Adam Csank's presentation at AAG 2019. Nguyen Tan Thai Hung is supported by the President's Graduate Fellowship from the Singapore University of Technology and Design. Chenxi Xu is supported by the Chinese Academy of Sciences (CAS) Pioneer Hundred Talents Program.

References

Borgomeo, E., Farmer, C. L., & Hall, J. W. (2015, jul). Numerical rivers: A synthetic streamflow generator for water resources vulnerability assessments. *Water Resources Research*, *51*(7), 5382–5405. DOI: 10.1002/2014WR016827

Borgomeo, E., Pflug, G., Hall, J. W., & Hochrainer-Stigler, S. (2015, nov). Assessing water resource system vulnerability to unprecedented hydrological drought using copulas to characterize drought duration and deficit. *Water Resources Research*, *51*(11), 8927–8948. DOI: 10.1002/2015WR017324

Buckley, B. M., Anchukaitis, K. J., Penny, D., Fletcher, R., Cook, E. R., Sano, M.,

... Hong, T. M. (2010, apr). Climate as a contributing factor in the demise of Angkor, Cambodia. *Proceedings of the National Academy of Sciences*, *107*(15), 6748–6752. DOI: 10.1073/pnas.0910827107

Buckley, B. M., Barbetti, M., Watanasak, M., Arrigo, R. D., Boonchirdchoo, S., & Sarutanon, S. (1995, feb). Dendrochronological Investigations in Thailand. *IAWA Journal*, *16*(4), 393–409. DOI: 10.1163/22941932-90001429

Buckley, B. M., Duangsathaporn, K., Palakit, K., Butler, S., Syhapanya, V., & Xaybouangeun, N. (2007, dec). Analyses of growth rings of Pinus merkusii from Lao P.D.R. *Forest Ecology and Management*, *253*(1-3), 120–127. DOI: 10.1016/j.foreco.2007.07.018

Buckley, B. M., Fletcher, R., Wang, S. Y. S., Zottoli, B., & Pottier, C. (2014). Monsoon extremes and society over the past millennium on mainland Southeast Asia. *Quaternary Science Reviews*, *95*, 1–19. DOI: 10.1016/j.quascirev.2014.04.022

Buckley, B. M., Palakit, K., Duangsathaporn, K., Sanguantham, P., & Prasomsin, P. (2007). Decadal scale droughts over northwestern Thailand over the past 448 years: Links to the tropical Pacific and Indian Ocean sectors. *Climate Dynamics*, *29*(1), 63–71. DOI: 10.1007/s00382-007-0225-1

Buckley, B. M., Stahle, D. K., Luu, H. T., Wang, S. Y., Nguyen, T. Q. T., Thomas, P., ... Nguyen, V. T. (2017). Central Vietnam climate over the past five centuries from cypress tree rings. *Climate Dynamics*, *48*(11-12), 3707–3723. DOI: 10.1007/s00382-016-3297-y

Buckley, B. M., Ummenhofer, C. C., D'Arrigo, R. D., Hansen, K. G., Truong, L. H., Le, C. N., & Stahle, D. K. (2019, sep). Interdecadal Pacific Oscillation reconstructed from trans-Pacific tree rings: 1350–2004 CE. *Climate Dynamics*, *53*(5-6), 3181–3196. DOI: 10.1007/s00382-019-04694-4

Byrd, R. H., Lu, P., Nocedal, J., & Zhu, C. (1995, sep). A Limited Memory Algorithm for Bound Constrained Optimization. *SIAM Journal on Scientific Computing*, *16*(5), 1190–1208. DOI: 10.1137/0916069

Cook, B. I., & Buckley, B. M. (2009, dec). Objective determination of monsoon season onset, withdrawal, and length. *Journal of Geophysical Research*, *114*(D23), D23109. DOI: 10.1029/2009JD012795

Cook, E. R., Anchukaitis, K. J., Buckley, B. M., D'Arrigo, R. D., Jacoby, G. C., & Wright, W. E. (2010, apr). Asian Monsoon Failure and Megadrought During the Last Millennium. *Science*, *328*(5977), 486–489. DOI: 10.1126/science.1185188

Coulthard, B., Smith, D. J., & Meko, D. M. (2016, mar). Is worst-case scenario streamflow drought underestimated in British Columbia? A multi-century perspective for the south coast, derived from tree-rings. *Journal of Hydrology*, *534*, 205–218. DOI: 10.1016/j.jhydrol.2015.12.030

D'Arrigo, R., Abram, N. J., Ummenhofer, C., Palmer, J., & Mudelsee, M. (2011, feb). Reconstructed streamflow for Citarum River, Java, Indonesia: linkages to tropical climate dynamics. *Climate Dynamics*, *36*(3-4), 451–462. DOI: 10.1007/s00382-009-0717-2

D'Arrigo, R., Barbett, M., Watanasak, M., Buckley, B. M., Krusic, P., Boonchirdchoo, S., & Sarutanon, S. (1997, jan). Progress in Dendroclimatic Studies of Mountain Pine in Northern Thailand. *IAWA Journal*, *18*(4), 433–444. DOI: 10.1163/22941932-90001508

D'Arrigo, R., Palmer, J., Ummenhofer, C. C., Kyaw, N. N., & Krusic, P. (2011). Three centuries of Myanmar monsoon climate variability inferred from teak tree rings. *Geophysical Research Letters*, *38*(24), 1–5. DOI: 10.1029/2011GL049927

Divakar, L., Babel, M., Perret, S., & Gupta, A. D. (2011, apr). Optimal allocation of bulk water supplies to competing use sectors based on economic criterion – An application to the Chao Phraya River Basin, Thailand. *Journal of Hydrology*, *401*(1-2), 22–35. DOI: 10.1016/j.jhydrol.2011.02.003

Duarte Silva, A. P. (2001, jan). Efficient Variable Screening for Multivariate Analysis. *Journal of Multivariate Analysis*, *76*(1), 35–62. DOI: 10.1006/jmva.2000.1920

Duarte Silva, A. P. (2002, nov). Discarding variables in a Principal Component Analysis: Algorithms for all-subsets comparisons. *Computational Statistics*, *17*(2), 251–271. DOI: 10.1007/s001800200105

Fritts, H. C. (1976). *Tree Rings and Climate*. London: Elsevier. DOI: 10.1016/B978-0-12-268450-0.X5001-0

Fritts, H. C., Blasing, T. J., Hayden, B. P., & Kutzbach, J. E. (1971, oct). Multivariate Techniques for Specifying Tree-Growth and Climate Relationships and for Reconstructing Anomalies in Paleoclimate. *Journal of Applied Meteorology*, *10*(5), 845–864. DOI: 10.1175/1520-0450(1971)010⟨0845:MTFSTG⟩2.0.CO;2

Furnival, G. M., & Wilson, R. W. (1974). Regressions by leaps and bounds. *Technometrics*, *16*(4), 499–511. DOI: 10.1080/00401706.1974.10489231

Gagen, M., McCarroll, D., Loader, N. J., & Robertson, I. (2011). Stable Isotopes in Dendroclimatology: Moving Beyond 'Potential'. In M. K. Hughes, T. W. Swetnam, & H. F. Diaz (Eds.), *Dendroclimatology: Progress and prospects* (pp. 147–172). Dordrecht: Springer Netherlands. DOI: 10.1007/978-1-4020-5725-0_6

Galelli, S., Humphrey, G. B., Maier, H. R., Castelletti, A., Dandy, G. C., & Gibbs, M. S. (2014, dec). An evaluation framework for input variable selection algorithms for environmental data-driven models. *Environmental Modelling and Software*, *62*, 33–51. DOI: 10.1016/j.envsoft.2014.08.015

Güner, H. T., Köse, N., & Harley, G. L. (2017). A 200-year reconstruction of Kocasu River (Sakarya River Basin, Turkey) streamflow derived from a tree-ring network. *International Journal of Biometeorology*, *61*(3), 427–437. DOI: 10.1007/s00484-016-1223-y

Hansen, K. G., Buckley, B. M., Zottoli, B., D'Arrigo, R. D., Nam, L. C., Van Truong, V., ... Nguyen, H. X. (2017, nov). Discrete seasonal hydroclimate reconstructions over northern Vietnam for the past three and a half centuries. *Climatic Change*, *145*(1-2), 177–188. DOI: 10.1007/s10584-017-2084-z

Hardman, G., & Reil, O. E. (1936). The Relationship between Tree-Growth and

Stream Runoff in the Truckee River Basin, California-Nevada. *Nevada Agricultural Experiment Station Bulletin No. 141*.

Herman, J. D., Zeff, H. B., Lamontagne, J. R., Reed, P. M., & Characklis, G. W. (2016, nov). Synthetic Drought Scenario Generation to Support Bottom-Up Water Supply Vulnerability Assessments. *Journal of Water Resources Planning and Management*, *142*(11), 04016050. DOI: 10.1061/(ASCE)WR.1943-5452.0000701

Hidalgo, H. G., Piechota, T. C., & Dracup, J. A. (2000, nov). Alternative principal components regression procedures for dendrohydrologic reconstructions. *Water Resources Research*, *36*(11), 3241–3249. DOI: 10.1029/2000WR900097

Holland, J. H. (1975). *Adaptation In Natural and Artificial Systems.* Ann Arbor, Michigan: The University of Michigan Press.

Josse, J., & Husson, F. (2016). missMDA: A Package for Handling Missing Values in Multivariate Data Analysis. *Journal of Statistical Software*, *70*(1). DOI: 10.18637/jss.v070.i01

Kohavi, R., & John, G. H. (1997, dec). Wrappers for feature subset selection. *Artificial Intelligence*, *97*(1-2), 273–324. DOI: 10.1016/s0004-3702(97)00043-x

Lieberman, V. (2003). *Strange Parallels: Volume 1, Integration on the Mainland: Southeast Asia in Global Context, c.800–1830.* Cambridge University Press. Retrieved from `https://books.google.com.sg/books?id=-01JisWpJbEC`

Lieberman, V., & Buckley, B. M. (2012). *The impact of climate on Southeast Asia, circa 950-1820: New findings* (Vol. 46) (No. 5). DOI: 10.1017/S0026749X12000091

Meko, D. M., & Woodhouse, C. A. (2011). Application of Streamflow Reconstruction to Water Resources Management. In M. K. Hughes, T. W. Swetnam, & H. F. Diaz (Eds.), *Dendroclimatology: Progress and prospects* (pp. 231–261). Dordrecht: Springer Netherlands. DOI: 10.1007/978-1-4020-5725-0_8

Meko, D. M., Woodhouse, C. A., Baisan, C. A., Knight, T., Lukas, J. J., Hughes, M. K., & Salzer, M. W. (2007, may). Medieval drought in the upper Colorado River Basin. *Geophysical Research Letters*, *34*(10), L10705. DOI: 10.1029/2007GL029988

Nash, J. E., & Sutcliffe, J. V. (1970, apr). River flow forecasting through conceptual models part I — A discussion of principles. *Journal of Hydrology*, *10*(3), 282–290. DOI: 10.1016/0022-1694(70)90255-6

Nguyen, H. T. T., & Galelli, S. (2018, mar). A Linear Dynamical Systems Approach to Streamflow Reconstruction Reveals History of Regime Shifts in Northern Thailand. *Water Resources Research*, *54*(3), 2057–2077. DOI: 10.1002/2017WR022114

Nguyen, H. T. T., Turner, S. W. D., Buckley, B. M., & Galelli, S. (2020, sep). Coherent stream flow variability in Monsoon Asia over the past eight centuries—links to oceanic drivers. *Water Resources Research*. DOI: 10.1029/2020WR027883

Pielke, R. A., Wilby, R., Niyogi, D., Hossain, F., Dairuku, K., Adegoke, J., ... Suding, K. (2012). Dealing With Complexity and Extreme Events Using a

Bottom-Up, Resource-Based Vulnerability Perspective. In *Extreme events and natural hazards: The complexity perspective* (pp. 345–359). American Geophysical Union. DOI: 10.1029/2011GM001086

Politis, D. N., & Romano, J. P. (1994). The Stationary Bootstrap. *Journal of the American Statistical Association*, *89*(428), 1303–1313. DOI: 10.1080/01621459.1994.10476870

Prairie, J., Nowak, K., Rajagopalan, B., Lall, U., & Fulp, T. (2008). A stochastic nonparametric approach for streamflow generation combining observational and paleoreconstructed data. *Water Resources Research*, *44*(6), 1–11. DOI: 10.1029/2007WR006684

Rao, M. P. (2020). *Hydroclimate variability and environmental change in Eurasia over the past millennium and its impacts* (PhD Thesis, Columbia University). DOI: 10.7916/d8-890y-wb66

Rao, M. P., Cook, E. R., Cook, B. I., Palmer, J. G., Uriarte, M., Devineni, N., ... Wahab, M. (2018, aug). Six Centuries of Upper Indus Basin Streamflow Variability and Its Climatic Drivers. *Water Resources Research*, *54*(8), 5687–5701. DOI: 10.1029/2018WR023080

Sano, M., Buckley, B. M., & Sweda, T. (2009). Tree-ring based hydroclimate reconstruction over northern Vietnam from Fokienia hodginsi: Eighteenth century mega-drought and tropical Pacific influence. *Climate Dynamics*, *33*(2-3), 331–340. DOI: 10.1007/s00382-008-0454-y

Sano, M., Xu, C., & Nakatsuka, T. (2012, jun). A 300-year Vietnam hydroclimate and ENSO variability record reconstructed from tree ring δ 18 O. *Journal of Geophysical Research: Atmospheres*, *117*(D12), D12115. DOI: 10.1029/2012JD017749

Sauchyn, D., & Ilich, N. (2017, nov). Nine Hundred Years of Weekly Streamflows: Stochastic Downscaling of Ensemble Tree-Ring Reconstructions. *Water Resources Research*, 1–18. DOI: 10.1002/2017WR021585

Schulman, E. (1945). Tree-ring hydrology of the Colorado River Basin. *University of Arizona Bulletin Series, Laboratory of Tree-Ring Research Bulletin No. 2*, *XVI*(4).

Scrucca, L. (2013). GA: A Package for Genetic Algorithms in R. *Journal of Statistical Software*, *53*(4), 1–37. DOI: 10.18637/jss.v053.i04

Stagge, J. H., Rosenberg, D. E., DeRose, R. J., & Rittenour, T. M. (2018). Monthly paleostreamflow reconstruction from annual tree-ring chronologies. *Journal of Hydrology*, *557*, 791–804. DOI: 10.1016/j.jhydrol.2017.12.057

Stockton, C. W. (1971). *The Feasibility of Augmenting Hydrologic Records using Tree-Ring Data* (PhD Thesis). University of Arizona.

Stockton, C. W., & Jacoby, G. C. (1976). Long-term Surface-water Supply and Streamflow Trends in the Upper Colorado River Basin Based on Tree-ring Analyses. *Lake Powell Research Project Bulletin 18*.

Treydte, K. S., Schleser, G. H., Helle, G., Frank, D. C., Winiger, M., Haug, G. H., & Esper, J. (2006, apr). The twentieth century was the wettest period in northern Pakistan over the past millennium. *Nature*, *440*(7088), 1179–1182. DOI:

10.1038/nature04743

Whitley, D. (1994, jun). A genetic algorithm tutorial. *Statistics and Computing*, *4*(2). DOI: 10.1007/BF00175354

Woodhouse, C. A., Gray, S. T., & Meko, D. M. (2006). Updated streamflow reconstructions for the Upper Colorado River Basin. *Water Resources Research*, *42*(5), W05415. DOI: 10.1029/2005WR004455

Xu, C., Buckley, B. M., Promchote, P., Wang, S. S., Pumijumnong, N., An, W., ... Guo, Z. (2019). Increased Variability of Thailand's Chao Phraya River Peak Season Flow and Its Association With ENSO Variability: Evidence From Tree Ring δ18O. *Geophysical Research Letters*, *46*(9), 4863–4872. DOI: 10.1029/2018GL081458

Xu, C., Pumijumnong, N., Nakatsuka, T., Sano, M., & Guo, Z. (2018). Inter-annual and multi-decadal variability of monsoon season rainfall in central Thailand during the period 1804–1999, as inferred from tree ring oxygen isotopes. *International Journal of Climatology*, *38*(15), 5766–5776. DOI: 10.1002/joc.5859

Xu, C., Pumijumnong, N., Nakatsuka, T., Sano, M., & Li, Z. (2015). A tree-ring cellulose δ18O-based July-October precipitation reconstruction since AD 1828, northwest Thailand. *Journal of Hydrology*, *529*(P2), 433–441. DOI: 10.1016/j.jhydrol.2015.02.037

Xu, C., Sano, M., & Nakatsuka, T. (2011, dec). Tree ring cellulose δ18O of Fokienia hodginsii in northern Laos: A promising proxy to reconstruct ENSO? *Journal of Geophysical Research: Atmospheres*, *116*(D24), D24109. DOI: 10.1029/2011JD016694

Xu, C., Sano, M., & Nakatsuka, T. (2013, sep). A 400-year record of hydroclimate variability and local ENSO history in northern Southeast Asia inferred from tree-ring δ18O. *Palaeogeography, Palaeoclimatology, Palaeoecology*, *386*, 588–598. DOI: 10.1016/j.palaeo.2013.06.025

Xu, G., Liu, X., Trouet, V., Treydte, K., Wu, G., Chen, T., ... Qin, D. (2019, jan). Regional drought shifts (1710–2010) in East Central Asia and linkages with atmospheric circulation recorded in tree-ring δ18O. *Climate Dynamics*, *52*, 713–727. DOI: 10.1007/s00382-018-4215-2

Zhu, M., Stott, L., Buckley, B. M., Yoshimura, K., & Ra, K. (2012, jun). Indo-Pacific Warm Pool convection and ENSO since 1867 derived from Cambodian pine tree cellulose oxygen isotopes. *Journal of Geophysical Research: Atmospheres*, *117*(D11), D11307. DOI: 10.1029/2011JD017198